Research Article

Feiying Sun, Changbin Nie, Xingzhan Wei, Hu Mao, Yupeng Zhang* and Guo Ping Wang

All-optical modulation based on MoS_2-Plasmonic nanoslit hybrid structures

https://doi.org/10.1515/nanoph-2021-0279
Received June 2, 2021; accepted October 4, 2021;
published online October 15, 2021

Abstract: Two-dimensional (2D) materials with excellent optical properties and complementary metal-oxide-semiconductor (CMOS) compatibility have promising application prospects for developing highly efficient, small-scale all-optical modulators. However, due to the weak nonlinear light-material interaction, high power density and large contact area are usually required, resulting in low light modulation efficiency. In addition, the use of such large-band-gap materials limits the modulation wavelength. In this study, we propose an all-optical modulator integrated Si waveguide and single-layer MoS_2 with a plasmonic nanoslit, wherein modulation and signal light beams are converted into plasmon through nanoslit confinement and together are strongly coupled to 2D MoS_2. This enables MoS_2 to absorb signal light with photon energies less than the bandgap, thereby achieving high-efficiency amplitude modulation at 1550 nm. As a result, the modulation efficiency of the device is up to 0.41 dB μm^{-1}, and the effective size is only 9.7 μm. Compared with other 2D material-based all-optical modulators, this fabricated device exhibits excellent light modulation efficiency with a micron-level size, which is potential in small-scale optical modulators and chip-integration applications. Moreover, the MoS_2-plasmonic nanoslit modulator also provides an opportunity for TMDs in the application of infrared optoelectronics.

***Corresponding author: Yupeng Zhang**, Institute of Microscale Optoelectronics, Shenzhen University, Shenzhen, 518060, People's Republic of China, E-mail: ypzhang@szu.edu.cn. https://orcid.org/0000-0003-2351-5579
Feiying Sun and Guo Ping Wang, Institute of Microscale Optoelectronics, Shenzhen University, Shenzhen, 518060, People's Republic of China
Changbin Nie and Xingzhan Wei, Chongqing Key Laboratory of Multi-scale Manufacturing Technology, Chongqing Institute of Green and Intelligent Technology, Chinese Academy of Sciences, Chongqing, 400714, People's Republic of China. https://orcid.org/0000-0003-4469-6639 (X. Wei)
Hu Mao, Guangdong Hongxin Technology Co. Ltd., Dongguan, 523690, People's Republic of China

Keywords: all-optical modulator; intraband transition; MoS_2; plasmonic nanoslit; waveguide.

1 Introduction

Photonic chip integration is an indispensable technology for information processing and communication. Critical components of this technology, such as lasers, detectors, and modulators, have been gaining increasing attention [1–3]. Among them, the all-optical modulators can completely convert and modulate signals in the optical domain which are essential for on-chip interconnection, short-distance communications [4, 5]. To implement their use in such applications, smaller-sized all-optical modulators are required, while sufficient modulation depth should be maintained. However, the all-optical devices based on traditional three-dimensional semiconductors, such as Si [6], lithium niobate [7], and III–V compound semiconductors [8], are usually limited in size to a few millimeters or centimeters duo to the inherent bulk material properties.

Owing to the atomic-level thickness, CMOS compatibility, and excellent optoelectronic properties, two-dimensional (2D) material-based hybrid nanophotonic components are a promising platform for realizing integrated optoelectronic or photonic devices. Among the emerging possibilities, all-optical modulators based on 2D materials have shown great potential [9–12]. In recent years, all-optical modulation with 2D materials such as graphene [13–19], transition metal dichalcogenides (TMDs) [20–23], and black phosphorous [24, 25] have been successively demonstrated based on nonlinear light saturation absorption effect [26, 27]. However, due to the low optical absorption of 2D materials arising from their atomic thickness, a high-power density and large light–matter interaction area are required to ensure that the device can achieve sufficiently large modulation depths (2–17 dB) [14–25], but that limits the modulation efficiency (only 10^{-2}–10^{-4} dB μm^{-1}). Furthermore, the strong light–matter interaction in most 2D materials (i.e., TMDs) lies in the visible range, restricting the applications in optical

communication wavelength bands [28]. Recently, TMDs that exceed the bandgap to achieve optical modulation have been individually reported owing to sub-bandgap transition [29, 30] caused by crystallographic defects or edge states [11, 25]. However, in such cases, the low transition efficiency results in insufficient light absorption and low modulation efficiency. A solution may be found in plasmonic nanoslit [31–34] which squeezes the light into a narrow mode with high electromagnetic confinement, not only ensures strong coupling between light and 2D materials but also compresses the device volume. In the previous work of graphene-slit waveguides, the modulation efficiency has been initially improved [34].

Herein, we fabricated an all-optical modulator with a monolayer MoS_2 and a plasmonic nanoslit hybrid structure. The strong field confinement at the nanoslit, for both the signal and modulation lights, is used to enhance the light–matter interaction dramatically and extend the operating wavelength range. With an effective size of only 9.7 μm, is successfully fabricated. Experimentally, the 532-nm modulation light facilitates effective control of the 1550 nm signal light, and the modulation efficiency is 0.41 dB μm^{-1}. This study expands the application of 2D TMDs materials with a large intrinsic bandgap in infrared optoelectronics, offering an opportunity for developing high-efficiency all-optical modulators based on 2D TMDs materials.

2 Main text

A schematic diagram of the MoS_2-plasmonic nanoslit all-optical modulator is shown in Figure 1a. The signal light (1550 nm) in the fiber is coupled to the Si waveguide and then converted to surface plasmon polaritons (SPPs) in the Au nanoslit due to the strong field confinement. The monolayer MoS_2, as a light-absorbing layer, is transferred to the surface of nanoslit to realize the strong interaction with the excited SPPs. Different from signal light, the modulation light (532 nm laser) is illuminated onto the MoS_2-plasmonic nanoslit hybrid structure in free space. Figure 1b shows the working mechanism of the proposed all-optical modulator. The off and on state of modulation light is depicted by the blue curve, while the corresponding changes of the signal light are shown in the red curve. When the 532 nm modulation light is in the OFF state, the signal light SPP cannot be absorbed by MoS_2 because its energy is less than the MoS_2 band gap (Figure 1b OFF state and Figure S1a). However, in the ON state of the modulation light, a large number of electron-hole pairs can be generated in MoS_2 (Figure 1b, ON state, i). The excited electrons can further interact with the signal light SPP and undergo an intraband transition (as shown in Figure 1b, ON state, ii) [35, 36]. As a result, the output intensity of signal light can be modulated effectively by switching the 532 nm laser.

According to the intraband transition theory and plasmon effect [37], the light absorption coefficient of the signal light SPP can be expressed as

$$\alpha = \frac{ne^2}{m^*\eta c\omega^2\epsilon_0\tau}. \quad (1)$$

where $m^\star$ is the effective mass of the electron, η is the refractive index of the MoS_2 film, ϵ_0 is the vacuum dielectric constant, w is the signal light angular frequency, τ is the electron relaxation time, e is the electron charge, and n is the carrier concentration (see Supplementary Note 2 for detailed formula derivation).

According to Equation (1), the absorption coefficient α is proportional to the square of the signal light wavelength and the carrier concentration. The carrier concentration depends on the intensity of the signal and modulation light. By changing the intensity of the modulation light, the light absorption coefficient of MoS_2 for the signal light SPP can be changed. Therefore, the transmission output of the signal light can be modulated by controlling the intensity of modulation light.

The influence of nanoslit width on the signal and modulation light confined fields was analyzed by the finite element analysis method. Figure 1c depicts the cross-sectional view of the MoS_2-plasmonic nanoslit structure in the *yz* direction. The plasmonic nanoslit is composed of Au and Si and has a width of *W*. In our previous study, this design meant that the refractive indexes of the upper and lower layers of the Au nanoslit were symmetrical (both the upper and lower layers are air), enabling the electromagnetic field to be better confined in the nanoslit [34]. Figure 1d shows the electric field distribution at the signal light in the nanoslit, which corresponds to the schematic structural diagram of Figure 1c (the white dashed line marks the position of the Au layer). The confined electric fields of the signal SPP are mainly distributed at the surface of Au nanoslit, which ensures that the MoS_2 can sufficiently interact with the electromagnetic field. Another beam of modulation light irradiates the nanoslit in the *xy* plane vertically, generating strong LSP resonance [38, 39], which further enhances the local electric field of the modulation light at the nanoslit (Figure 1e).

The electric field energy at the contact interface for the plasmon formed by the two beams of light and MoS_2 is plotted as a function of slit width in Figure 1f (electric field

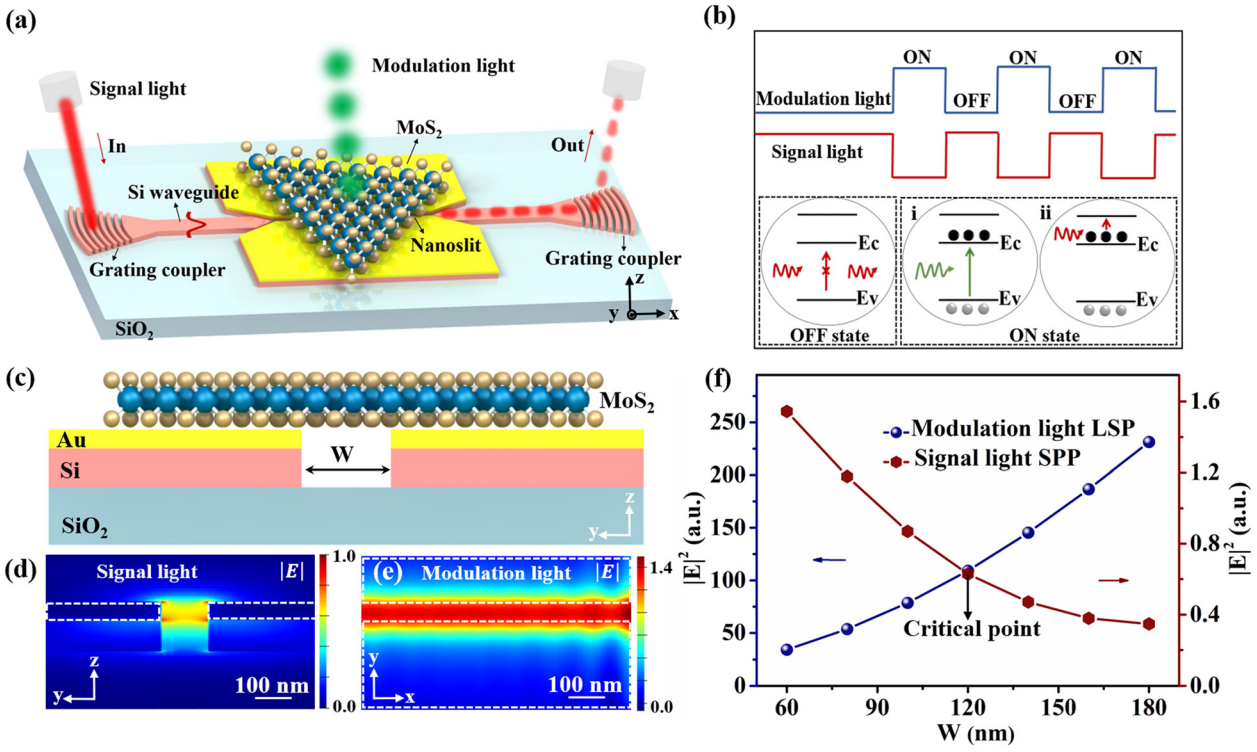

Figure 1: MoS_2-plasmonic nanoslit all-optical modulation.
(a) Schematic diagram of the device structure. (b) Working principle of the all-optical modulation. (c) Cross-sectional view of (a) (in *yz* plane). (d)–(e) Confined electric field distribution of signal and modulation lights. The slot width is 120 nm in each case, and the Au and Si layer thickness are 80 and 140 nm, respectively. Scale bar, 100 nm. The wavelengths of the signal and modulation lights are set to 1550 and 532 nm, respectively. And the TE mode is selected. (f) Electric-field energy of signal light SPP and modulation light LSP as functions of plasmonic nanoslit width.

energy: $E^2 = \int |E_i|^2 \, dw$, where E_i is the electric field intensity at the point of contact between the nanoslit and MoS_2, and W is the width of the nanoslit). The trends for the two curves are exactly opposite: the electric field intensity of the signal light SPP decreases exponentially with nanoslit width, while the modulation light LSP gradually increases. This is due to the different resonance frequencies and excitation mode of the modulation and signal light. It is revealed that for the signal light, the smaller nanoslit has a strong confined field, which can improve the SPP–MoS_2 interaction. For the modulation light, a large nanoslit width can ensure that a larger proportion of LSP are absorbed by MoS_2. In addition, the electric field energy of the modulation light LSP is much higher than that of the signal light SPP, which means that the influence of the modulation light LSP on the device performance will be dominant. To satisfy the requirement for sufficient interaction between the plasmon and MoS_2, a trade-off is required to select a suitable nanoslit width. The 120-nm slit width is considered as the critical point, at which the electric field intensities of the signal and modulation light plasmon are completely balanced. Therefore, this is regarded as the optimal slit width.

The material properties of MoS_2 and the prepared MoS_2-plasmonic nanoslit device were characterized. A micrograph of the MoS_2 grown on the SiO_2 substrate is shown in Figure 2a. The MoS_2 film is triangular and has a uniform thickness. The length of this MoS_2 section is approximately 100 μm (white dotted line) and can be positioned to completely cover the nanoslit by use of the directional transfer method. Scanning transmission electron microscopy (STEM) allowed observation of the regular atomic structure of MoS_2 (Figure 2b). The selected area electron diffraction (SAED) pattern (the inset in Figure 2b) reveals the single crystal characteristics of MoS_2. Figure 2c depicts the Raman spectrum of MoS_2, with peaks assigned to the in-plane E^1_{2g} mode and the out-of-plane A_{1g} mode at 384.6 and 404 cm^{-1}, respectively. The frequency difference between the two modes is approximately 20 cm^{-1}, indicating that the MoS_2 forms a monolayer on the surface [40]. The photoluminescence (PL) spectrum of MoS_2 (the inset in Figure 2c) shows that its optical band gap is 1.84 eV [41],

consistent with the theoretically reported monolayer MoS_2 band gap (1.8 eV). A false-color SEM image of the MoS_2-plasmonic nanoslit device is given in Figure 2d (detailed device preparation is given in Supplementary Note 3). The MoS_2 film, highlighted by a dark green color, completely covers the plasmonic nanoslit region. The length of the nanoslit is 9.7 μm, and the width is 120 nm. The propagation loss of the plasmonic nanoslit is estimated to be approximately 5 dB. The atomic force microscopy (AFM) amplitude map shows that the MoS_2 film on the nanoslit is undamaged (Figure 2e), and the height scan of the white dashed area shows the MoS_2 is suspended on the nanoslit, ensuring that the MoS_2 can fully interact with the confined electric field in the nanoslit. In addition, the typical Raman peak intensities for different slit widths are shown in Figure 2f. The wavelength of the laser light source used is 523 nm and the microscope magnification is 100×. The results show that the Raman typical peak intensity is highest when the slit width is 120 nm. This reveals that with 532-nm excitation, the larger the nanoslit width, the stronger the electromagnetic enhancement caused by LSP resonance. This conclusion verifies the simulation results for the MoS_2-plasmonic nanoslit with modulation-light excitation.

The MoS_2-plasmonic nanoslit all-optical experiment was conducted to verify the modulation ability. The optical test system used in the experiment is shown in Figure 3a. The output wavelength of the tunable continuous laser (TFL-C-20) is 1550 nm (power, 1 mW), and this is used as the signal light. The fiber polarization controller is used to select TE-mode light as the signal light and couple it to the device through a tapered fiber. At the other end of the output, the spectrum analyzer is connected to the optical fiber (AQ6370D, wavelength range: 600–1700 nm) to receive the signal light. The insertion loss of the device was 42 dB, mainly from the fiber-waveguide coupling and the signal light SPPs propagation in nanoslit. A 532-nm laser is used as the modulation light with a 160-μm spot diameter, and the maximum output power is 80 mW. By adjusting the rotation angle of the attenuator, modulation light output with different powers can be realized. Figure 3b depicts the signal light transmission output ($T = 10 \times \log10(P_{out}/P_{in})$), where P_{in} is the signal light input power and P_{out} is the signal light output power as a function of the modulation light power. When the modulation is in the OFF state, the signal light output intensity is −48.4 dBm. As the modulation light power increases, the signal light output intensity gradually decreases, indicating that the absorption of signal light by MoS_2 increases.

The blue curve in Figure 3c is the signal light transmission output at 1550 nm and this decreases linearly as the power increases. This trend is exactly the opposite of that for light saturation absorption in all-optical

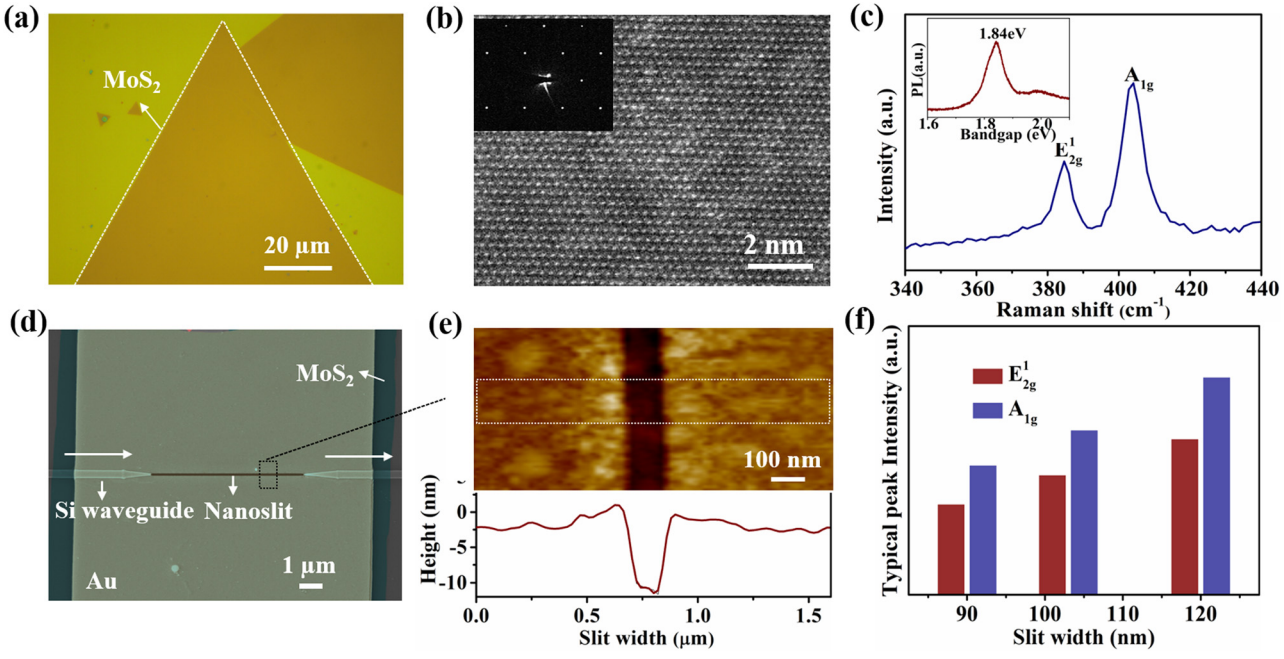

Figure 2: MoS_2 material and MoS_2-plasmonic nanoslit device characterization.
(a) Microscopy image of MoS_2 thin film grown on SiO_2. (b) STEM image of MoS_2 crystal; the inset shows the SAED pattern. (c) Raman and PL spectrum of monolayer MoS_2. (d) False-color SEM image of the device. (e) Amplitude scan of MoS_2-plasmonic nanoslit area by AFM; the height difference between the MoS_2 film at the nanoslit and the Au surface is approximately 7 nm. (f) Typical Raman peak intensities of MoS_2 with slit widths of 120, 100, and 90 nm.

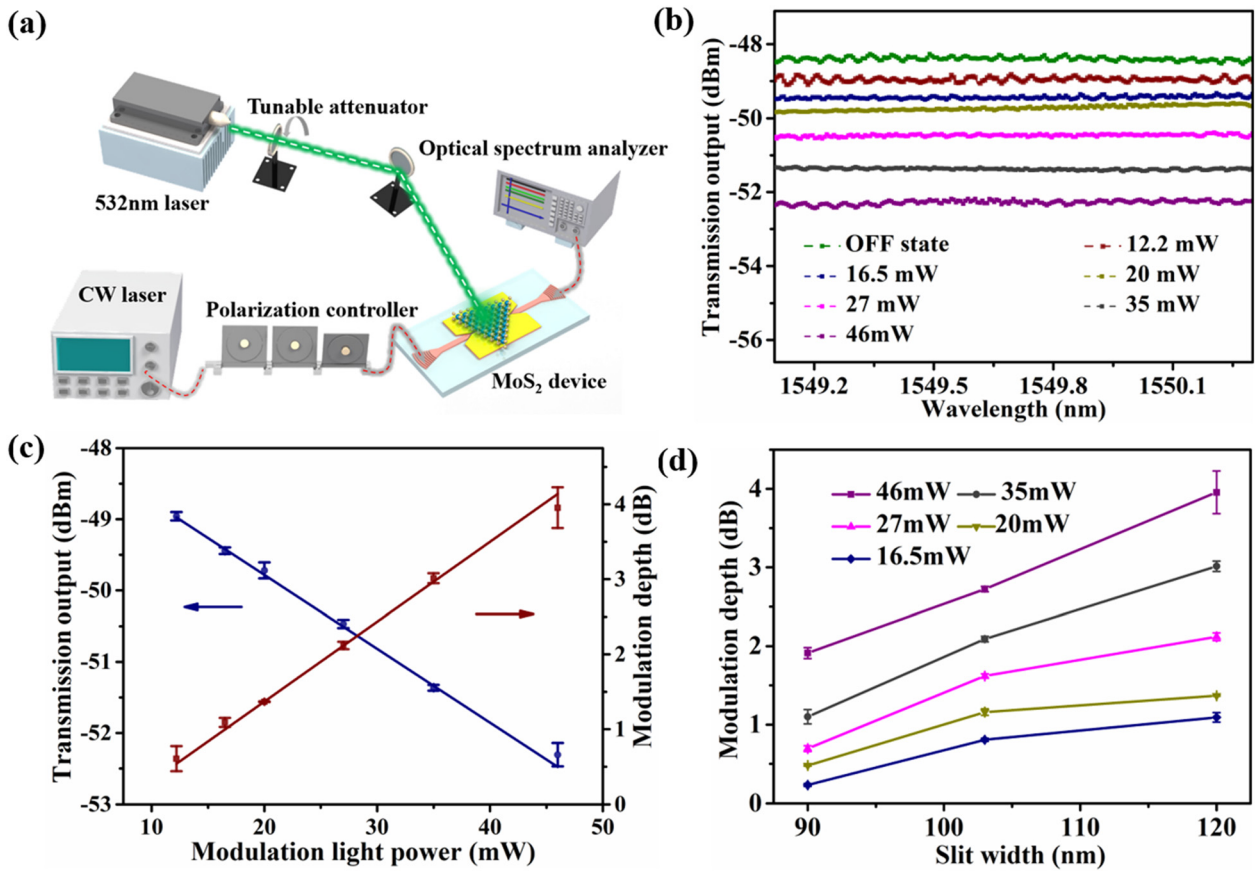

Figure 3: MoS_2-plasmonic nanoslit device all-optical modulation.
(a) All-optical modulation test system. (b) Change in signal light output with modulation light power. (c) Transmission output (T(dBm) = 10 × log10(P_{out}/1 mW)) and modulation depth of the signal light. (d) Modulation depth as a function of slit width; the slit widths are 90, 110, and 120 nm.

modulation because the increase in modulation light power stimulates MoS_2 to generate more localized electron–hole pairs, leading to intraband electron transitions that require the absorption of a larger amount of signal SPPs. However, for optical saturable absorption modulators, Pauli blocking causes photon competition between the signal and modulation light. Consequently, the absorption of the signal light decreases when the power of modulation light increases [13]. The modulation depth, represented by the red curve in Figure 3c, increases linearly as the modulation power since it is proportional to the modulation light-induced absorption coefficient. The maximum modulation depth is 3.95 dB, and the modulation efficiency (modulation efficiency = modulation depth/effective contact length) is 0.41 dB/μm. When the modulation light power increased, the output of signal light would increase correspondingly, and eventually tend to be saturated. This is caused by the energy threshold of the material.

The modulation depths of the devices with nanoslit widths of 90 and 103 nm were also tested (Figure 3d). Under the same laser power, their maximum modulation depths are 1.9 and 2.7 dB, respectively. Among the devices with nanoslit widths of 90, 103, and 120 nm, the 120-nm-width device has the largest modulation depth (3.95 dB). This reveals that the influence of the nanoslit width on the modulation light LSP plays a dominant role in determining the modulation depth of the device, within a certain width range, which verifies the theoretical simulation results. It is also demonstrated that the device modulation is not caused by direct excitation of the signal light SPP, nor is it a result of a thermal effect of the signal light irradiation. In addition, we also fabricated a normal silicon waveguide device with MoS_2, where the area of MoS_2 was the same as that of the nanoslit device. Under the maximum power excitation (46 mW), the experimental result shows that the light-induced absorption at 1550 nm is almost weak (as shown in Figure S4).

To further verify the MoS_2 all-optical modulation mechanism excited by the plasmonic nanoslit, an experiment based on the double-layer MoS_2 all-optical modulator

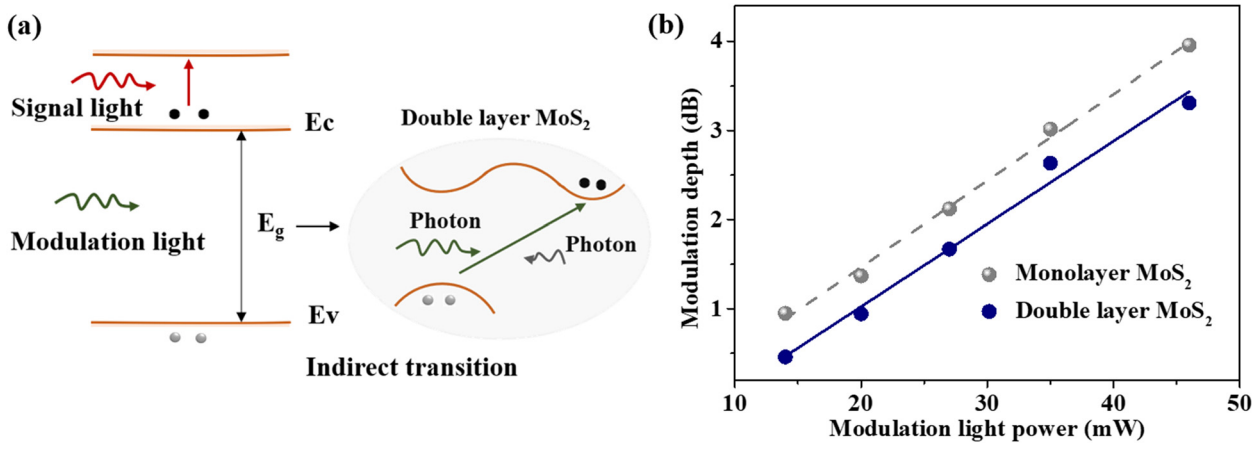

Figure 4: Double-layer MoS_2-plasmonic nanoslit all-optical modulation.
(a) Schematic of working principle for the double-layer MoS_2 device. (b) Modulation depth of monolayer and double-layer MoS_2 devices versus modulation light power.

was performed. Unlike monolayer MoS_2 which has a direct bandgap, double-layer MoS_2 is an indirect-band-gap material. The interband transition not only requires the interaction of photons and electrons but also depends on the participation of phonons (Figure 4a). This leads to a transition probability lower than that of a direct transition when the modulation light LSP is excited [42, 43]. Therefore, the number of electron–hole pairs generated by the double-layer MoS_2 via excitation by the modulation light LSP is significantly reduced, leading to a reduction in the signal light absorption. The double-layer MoS_2-plasmonic nanoslit device was prepared with a slit width of 120 nm (other parameters are the same as mentioned above). The results in Figure 4b show that the modulation depth of the double-layer MoS_2 device is obviously lower than that of the single-layer device, at the same modulation light intensity. The modulation depth of the double-layer MoS_2 device is 3.3 dB, and the modulation efficiency is 0.34 dB μm^{-1}. This result further confirms the modulation mechanism of the device and also proves that it is not caused by a thermal effect of the metal.

The dynamic response mechanism of the proposed modulator is characterized and analyzed next (Figure 5). For the MoS_2-plasmonic nanoslit hybrid structure, the work function mismatch between MoS_2 and Au structure leads to the Fermi level of MoS_2 shift (Figure 5a i–ii) [44–46] and the formation of a homojunction of MoS_2 with a symmetrical built-in electric field (Figure 5a ii–iii). When the modulation light is illuminated, the excited electrons in the depletion region will move to the center of nanoslit (Figure 5a iii) and interact with the signal light SPP to undergo an intraband transition. The output signal light intensity thereby decreases gradually until the internal electric field of MoS_2 reaches dynamic balance. When the modulation light is turned off, the photogenerated carriers will overcome the built-in electric field and gradually recombine to the initial equilibrium state. Therefore, the response time of the proposed modulator depends on the photocarrier dynamics in the MoS_2-plasmonic nanoslit hybrid structure.

The response time test of the proposed modulator is carried out, and the experimental setup is shown in Figure S5. A square-wave control light (wavelength is 532 nm) with a modulation frequency of 10–5000 Hz and optical power of 30 mW is coupled into the MoS_2-plasmonic nanoslit hybrid structure. The output signal is received by a 5 GHz photodetector and a 100 MHz oscilloscope. Figure 5b shows the waveforms of signal output at the modulation frequency of 10 Hz. The results signify that the rise time is about 11 ms and the fall time is about 14 ms (Figure 5c). The change of output voltage ($V_{max} - V_{min}$) at different frequencies is shown in Figure 5d. The 3 dB bandwidth [47] of the MoS_2-plasmonic nanoslit modulator is estimated to be 700 Hz. Compared with most TMDs' all-optical modulators, our modulator shows an excellent frequency response [20, 30].

For the proposed device structure, both the signal and modulation light can interact with MoS_2 by means of strong electromagnetic confinement of plasmonic nanoslit. Meanwhile, the drive of the built-in electric field in the homojunction makes the light–matter interaction area extend effectively. As a result, the proposed modulator exhibits higher modulation efficiency and smaller device size compared to the currently reported 2D material-based all-optical modulators (Table 1). In addition, the response time in the millisecond range is consistent with the currently reported TMDs based all-optical modulators

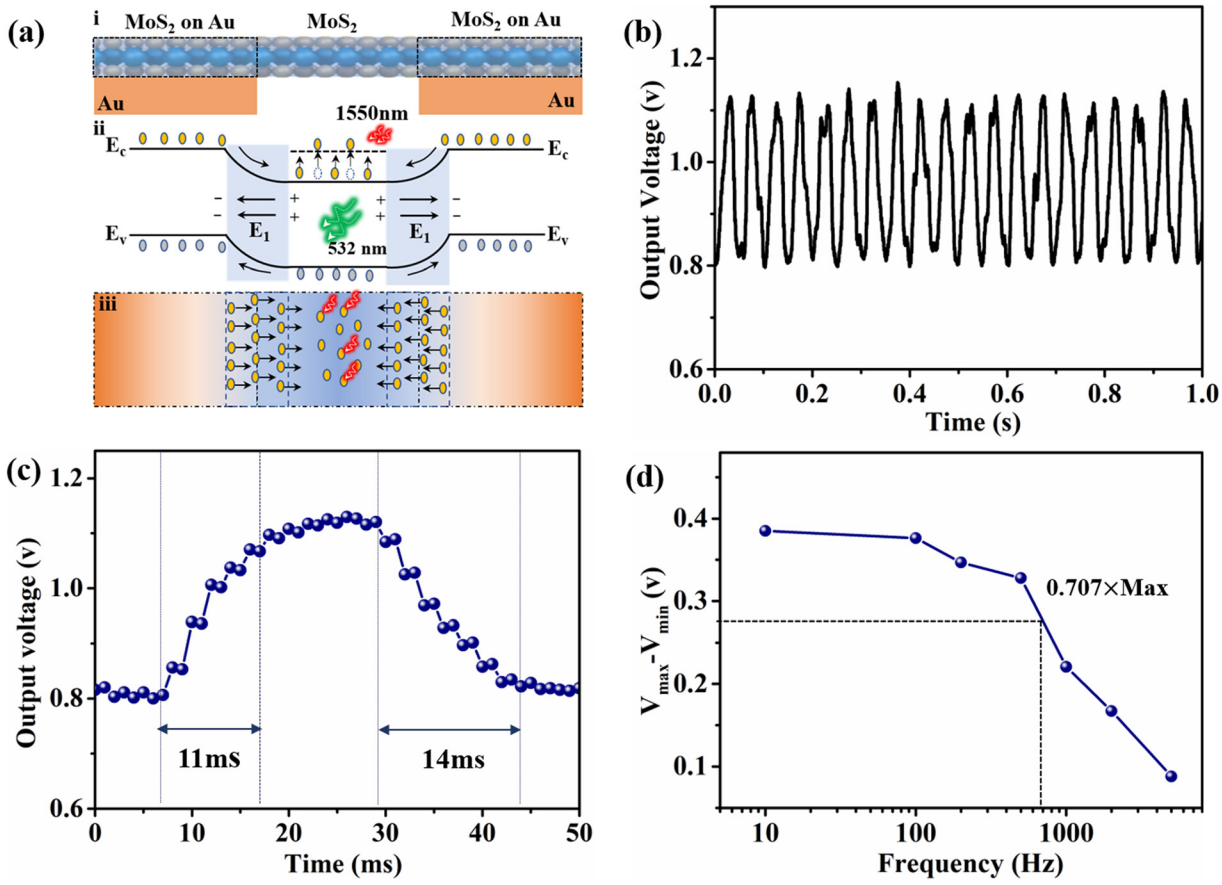

Figure 5: Frequency response of MoS_2-plasmonic nanoslit modulator.
(a) Schematic of dynamic response mechanism. (i) On both sides of the nanoslit, MoS_2 is in contact with the Au layer; on the nanoslit, MoS_2 is suspended. (ii) Energy band diagram of MoS_2 homojunction. (iii) Excited electron movement driven by a built-in electric field. (b) Measured signal light waveform changes with time. (c) Rise time and fall time of proposed modulator. (d) Output voltage changes at different frequencies.

[20, 30], even if the carrier dynamics in the homojunction cause the response time to be limited. Energy band engineering [48] or interface optimization technology [49] is expected to further balance the response time and the modulation efficiency, achieving a fast and high efficiency all-optical modulator.

Table 1: 2D material-based all-optical modulators.

Devices	Signal light (nm)	Modulation depth (dB)	Interaction length (μm)	Modulation efficiency (dB μm^{-1})	Rise time/fall time	Ref.
MoS_2-plasmonic nanoslit	1550	3.95	9.7	0.41	11/14 ms	This work
Optically induced MoS_2 nanosheets	632.8	7	–	–	–	[22]
WS_2/silicon-nitride waveguide	640	2	~50	~0.04	0.5/0.5 ms	[21]
$MoSe_2$-microfiber	1550	2	2.5×10^4	0.0012	400/600 ms	[30]
WS_2-microfiber	1520–1620	2.71–3.99	–	–	20.5/19.6 ms	[20]
Stereo graphene-microfiber	1550	7.5	12×10^3	6.3×10^{-4}	Ns	[15]
Graphene-clad microfiber	1550	38%	16	–	2.2 ps	[14]
Graphene-plasmonic slot	1550	2.1	10	0.21	–	[34]
Graphene plasmon-enhanced	1550	3.5	12	0.28	30–120 fs	[18]

3 Conclusions

In conclusion, we have realized the all-optical modulation using MoS_2 at 1550 nm via highly confined plasmonic nanoslit excitation. The maximum modulation efficiency can reach 0.41 dB μm^{-1} and the 3 dB bandwidth is about 700 Hz. Plasmonic nanoslit excitation in MoS_2 can be further extended to other 2D material optoelectronic devices. Furthermore, the small-scale MoS_2 optical modulator operates at the communication wavelength and is compatible with CMOS technology, which is suitable for the development of high-density integrated chips. This has great application prospects in on-chip optical interconnection and smart sensing.

Author contributions: All the authors have accepted responsibility for the entire content of this submitted manuscript and approved submission.

Research funding: This work was supported by the National Natural Science Foundation of China (NSFC) (61975134, 62005182), the Science and Technology Innovation Commission of Shenzhen (JCYJ20180305125345378), Guangdong Basic and Applied Basic Research Foundation (2020B1515020051), the Shenzhen Nanshan District Pilotage Team Program (LHTD20170006), Open Research Fund of State Key Laboratory of Laser-Matter Interaction (SKLLIM1901), and the State Key Research Development Program of China (2019YFB2203503).

Conflict of interest statement: The authors declare no conflicts of interest regarding this article.

References

[1] J. Ahn, M. Fiorentino, R. G. Beausoleil, N. Binkert, A. Davis, and D. Fattal, "Devices and architectures for photonic chip-scale integration," *Appl. Phys. A*, vol. 95, p. 989, 2009.

[2] R. Soref, "The past, present, and future of silicon photonics," *IEEE J. Sel. Top. Quant. Electron.*, vol. 12, p. 1678, 2006.

[3] H. T. Lin, Z. Q. Luo, T. Gu, et al., "Mid-infrared integrated photonics on silicon: a perspective," *Nanophotonics*, vol. 7, p. 393, 2017.

[4] T. K. Liang, L. R. Nunes, T. Sakamoto, K. Sasagawa, T. Kawanishi, and M. Tsuchiya, "Ultrafast all-optical switching by cross-absorption modulation in silicon wire waveguides," *Opt. Express*, vol. 13, p. 7298, 2005.

[5] A. Martínez, J. Blasco, P. Sanchis, J. Galán, J. G. Rupérez, and E. Jordana, "Ultrafast all-optical switching in a silicon-nanocrystal-based silicon slot waveguide at telecom wavelengths," *Nano Lett.*, vol. 10, p. 1506, 2010.

[6] H. K. Tsang, C. S. Wong, T. K. Liang, et al., "Optical dispersion, two-photon absorption and self-phase modulation in silicon waveguides at 1.5 μm wavelength," *Appl. Phys. Lett.*, vol. 80, p. 416, 2002.

[7] G. Singh, R. P. Yadav, and V. Janyani, "Ti indiffused Lithium Niobate (Ti: $LiNbO_3$) Mach-Zehnder interferometer all optical switches: a review," in *New Advanced Technologies*, A. Lazinica, Ed., London, United Kingdom, IntechOpen, 2010.

[8] P. Boucaud, P. Vagos, F. H. Julien, and J. M. Lourtioz, "Modulation bandwidth enhancement of all-optical modulators based on photo-induced intersub-band absorption in GaAs/AlGaAs quantum wells by proton bombardment," *Electron. Lett.*, vol. 28, p. 1373, 1992.

[9] K. S. Novoselov, V. I. Fal'ko, L. Colombo, P. R. Gellert, M. G. Schwab, and K. Kim, "A roadmap for graphene," *Nature*, vol. 490, p. 192, 2012.

[10] S. Z. Butler, S. M. Hollen, L. Y. Cao, Y. Cui, J. A. Gupta, and H. R. Gutiérrez, "Progress, challenges, and opportunities in two-dimensional materials beyond graphene," *ACS Nano*, vol. 7, p. 2898, 2013.

[11] N. R. Rao, A. K. Sood, K. S. Subrahmanyam, and A. Govindaraj, "Graphene: the new two-dimensional nanomaterial," *Angew. Chem. Int. Ed.*, vol. 48, p. 7752, 2009.

[12] Y. H. Yao, Z. Cheng, J. J. Dong, and X. L. Zhang, "Performance of integrated optical switches based on 2D materials and beyond," *Front. Optoelectron.*, vol. 13, p. 129, 2020.

[13] C. Y. Zhong, J. Y. Li, and H. T. Lin, "Graphene-based all-optical modulators," *Front. Optoelectron.*, vol. 13, p. 114, 2020.

[14] W. Li, B. G. Chen, C. Meng, W. Fang, and Y. Xiao, "Ultrafast all-optical graphene modulator," *Nano Lett.*, vol. 14, p. 955, 2014.

[15] J. H. Chen, B. C. Zheng, G. H. Shao, S. J. Ge, F. Xu, and Y. Q. Lu, "An all-optical modulator based on a stereo graphene-microfiber structure," *Light Sci. Appl.*, vol. 4, p. e360, 2015.

[16] F. Y. Sun, L. P. Xia, C. B. Nie, J. Shen, and Y. X. Zou, "The all-optical modulator in dielectric-loaded waveguide with graphene-silicon heterojunction structure," *Nanotechnology*, vol. 29, p. 135201, 2018.

[17] H. Wang, N. Yang, L. M. Chang, C. B. Zhou, S. Y. Li, and M. Deng, "CMOS-compatible all-optical modulator based on the saturable absorption of graphene," *Photonics Res.*, vol. 8, p. 468, 2020.

[18] M. Al Aloul and M. Rasras, "Low insertion loss plasmon-enhanced graphene all-optical modulator," *ACS Omega*, vol. 6, p. 7576, 2021.

[19] H. J. Zhang, N. Healy, L. Shen, C. C. Huang, D. W. Hewak, and A. C. Peacock, "Enhanced all-optical modulation in a graphene-coated fibre with low insertion loss," *Sci. Rep.*, vol. 6, p. 1, 2016.

[20] H. A. Li, Z. J. Huang, Y. W. Lang, X. L. Wang, H. Zhu, and Z. R. Shen, "Broadband all-light-control with WS_2 coated microfibers," *Opt. Express*, vol. 27, p. 12817, 2019.

[21] S. Yang, D. C. Liu, Z. L. Tan, K. Liu, Z. H. Zhu, and S. Q. Qin, "CMOS-compatible WS_2-based all-optical modulator," *ACS Photonics*, vol. 5, p. 342, 2018.

[22] N. N. Dong, Y. X. Li, S. F. Zhang, X. Y. Zhang, and J. Wang, "Optically induced transparency and extinction in dispersed MoS_2, $MoSe_2$, and graphene nanosheets," *Adv. Opt. Mater.*, vol. 5, p. 1700543, 2017.

[23] M. Liu, Z. W. Wei, A. P. Luo, W. C. Xu, and Z. C. Luo, "Recent progress on applications of 2D material-decorated microfiber photonic devices in pulse shaping and all-optical signal processing," *Nanophotonics*, vol. 9, p. 2641, 2020.

[24] Y. Z. Wang, F. Zhang, X. Tang, et al., "All-optical phosphorene phase modulator with enhanced stability under ambient conditions," *Laser Photonics Rev.*, vol. 12, p. 1800016, 2018.

[25] J. L. Zheng, X. Tang, Z. H. Yang, Z. M. Liang, and Y. X. Chen, "Few-Layer phosphorene-decorated microfiber for all-optical thresholding and optical modulation," *Adv. Opt. Mater.*, vol. 5, p. 1700026, 2017.
[26] K. P. Wang, Y. Y. Feng, C. X. Chang, J. X. Zhan, C. W. Wang, and Q. Z. Zhao, "Broadband ultrafast nonlinear absorption and nonlinear refraction of layered molybdenum dichalcogenide semiconductors," *Nanoscale*, vol. 6, p. 10530, 2014.
[27] J. D. Marini, F. J. Cox, and G. de Abajo, "Theory of graphene saturable absorption," *Phys. Rev. B*, vol. 95, p. 125408, 2017.
[28] Z. Sun, A. Martinez, and F. Wang, "Optical modulators with 2D layered materials," *Nat. Photonics*, vol. 10, p. 227, 2016.
[29] P. G. Yan, A. J. Liu, Y. S. Chen, H. Chen, S. C. Ruan, and C. Y. Guo, "Microfiber-based WS_2-film saturable absorber for ultra-fast photonics," *Opt. Mater. Express*, vol. 5, p. 479, 2015.
[30] H. Y. G. Zhang, W. G. Zhu, J. H. Yu, H. H. Lu, W. T. Qiu, and J. L. Dong, "All light-control-light properties of molybdenum diselenide ($MoSe_2$)-coated-microfiber," *Opt. Express*, vol. 25, p. 28536, 2017.
[31] A. Phatak, Z. Cheng, and C. Qin, "Design of electro-optic modulators based on graphene-on-silicon slot waveguides," *Opt. Lett.*, vol. 41, p. 2501, 2016.
[32] Z. Lu and W. Zhao, "Nanoscale electro-optic modulators based on graphene-slot waveguides," *JOSA B*, vol. 29, p. 1490, 2012.
[33] C. Huck, J. Vogt, and M. Sendner, "Plasmonic enhancement of infrared vibrational signals: nanoslits versus nanorods," *ACS Photonics*, vol. 2, p. 1489, 2015.
[34] F. Y. Sun, L. P. Xia, C. B. Nie et al., "An all-optical modulator based on a graphene–plasmonic slot waveguide at 1550 nm," *Appl. Phys. Express*, vol. 12, p. 042009, 2019.
[35] D. Pacifici, H. J. Lezec, and H. A. Atwater, "All-optical modulation by plasmonic excitation of CdSe quantum dots," *Nat. Photonics*, vol. 1, p. 402, 2007.
[36] V. I. Klimov, C. J. Schwarz, and D. W. McBranch, "Ultrafast dynamics of inter-and intraband transitions in semiconductor nanocrystals: implications for quantum-dot lasers," *Phys. Rev. B*, vol. 60, p. R2177, 1999.
[37] X. C. Shen, *Semiconductor Spectroscopy and Optical Properties*, Beijing, China, Scientific, 2002.
[38] Z. Z. Ma, K. Kikunaga, H. Wang, and S. Sun, "Compact graphene plasmonic slot photodetector on silicon-on-insulator with high responsivity," *ACS Photonics*, vol. 7, p. 932, 2020.
[39] S. A. Maier, *Plasmonics: Fundamentals and Applications*, New York, USA, Springer Science & Business Media, 2007.
[40] W. Chen, J. Zhao, J. Zhang, et al., "Oxygen-assisted chemical vapor deposition growth of large single-crystal and high-quality monolayer MoS_2," *J. Am. Chem. Soc.*, vol. 137, p. 15632, 2015.
[41] P. F. Yang, X. L. Zou, Z. P. Zhang, et al., "Batch production of 6-inch uniform monolayer molybdenum disulfide catalyzed by sodium in glass," *Nat. Commun.*, vol. 9, p. 1, 2018.
[42] M. Tamulewicz, J. K. Girzycka, K. Gajewski, J. Serafińczuk, and A. Sierakowski, "Layer number dependence of the work function and optical properties of single and few layers MoS_2: effect of substrate," *Nanotechnology*, vol. 30, p. 245708, 2019.
[43] K. F. Mak, C. G. Lee, J. Hone, J. Shan, and T. F. Heinz, "Atomically thin MoS_2: a new direct-gap semiconductor," *Phys. Rev. Lett.*, vol. 105, p. 136805, 2010.
[44] N. Kaushik, A. Nipane, and F. Basheer, "Schottky barrier heights for Au and Pd contacts to MoS_2," *Appl. Phys. Lett.*, vol. 105, p. 113505, 2014.
[45] Y. Katagiri, T. Nakamura, and A. Ishii, "Gate-tunable atomically thin lateral MoS_2 Schottky junction patterned by electron beam," *Nano Lett.*, vol. 16, p. 3788, 2016.
[46] X. Liu, F. Li, and M. Xu, "High response, self-powered photodetector based on the monolayer MoS_2/P–Si heterojunction with asymmetric electrodes," *Langmuir*, vol. 34, p. 14151, 2018.
[47] M. Kumar, M. Patel, and H. S. Kim, "High-speed, self-biased broadband photodetector-based on a solution-processed Ag nanowire/Si Schottky junction," *ACS Appl. Mater. Interfaces*, vol. 9, p. 38824, 2017.
[48] J. Li and D. Chu, "Energy band engineering of metal oxided for enhanced visible light absorption," in *Multifunctional photocatalytic materials for energy*, Z. Lin, M. Ye, and M. Wang, Eds., Netherlands, Elsevier, 2018, pp. 49–78.
[49] Y. Liu, J. Guo, and E. Zhu, "Approaching the Schottky–Mott limit in van der Waals metal–semiconductor junctions," *Nature*, vol. 557, p. 696, 2018.

Supplementary Material: The online version of this article offers supplementary material (https://doi.org/10.1515/nanoph-2021-0279).